

MEFNet: Multi-scale Event Fusion Network for Motion Deblurring

Lei Sun^{1,2}, Christos Sakaridis², Jingyun Liang², Qi Jiang¹, Kailun Yang³, Peng Sun¹, Yaozu Ye¹, Kaiwei Wang¹, and Luc Van Gool^{2,4}

¹ Zhejiang University ² ETH Zürich ³ Karlsruhe Institute of Technology ⁴ KU Leuven

Abstract

Traditional frame-based cameras inevitably suffer from motion blur due to long exposure times. As a kind of bio-inspired camera, the event camera records the intensity changes in an asynchronous way with high temporal resolution, providing valid image degradation information within the exposure time. In this paper, we rethink the event-based image deblurring problem and unfold it into an end-to-end two-stage image restoration network. To effectively utilize event information, we design (i) a novel symmetric cumulative event representation specifically for image deblurring, and (ii) an affine event-image fusion module applied at multiple levels of our network. We also propose an event mask gated connection between the two stages of the network so as to avoid information loss. At the dataset level, to foster event-based motion deblurring and to facilitate evaluation on challenging real-world images, we introduce the High-Quality Blur (HQBlur) dataset, captured with an event camera in an illumination-controlled optical laboratory. Our Multi-Scale Event Fusion Network (MEFNet) sets the new state of the art for motion deblurring, surpassing both the prior best-performing image-based method and all event-based methods with public implementations on the GoPro (by up to 2.38dB) and HQBlur datasets, even in extreme blurry conditions. Source code and dataset will be made publicly available.

1. Introduction

Motion blur often occurs in images due to camera shaking or object motion during the exposure time of the camera. The goal of deblurring is to recover a sharp image with clear edge structures and texture details from the blurry image. This is a highly ill-posed problem because of the infinitely many feasible solutions [2, 8, 50] and it has been an important task in low-level vision. Traditional methods explicitly utilize natural image priors and various constraints [2, 10, 16, 17, 21, 22, 46]. To better generalize when addressing the deblurring problem, modern learning-based methods choose to train Convolutional Neural Networks

(CNNs) on large-scale data to learn the implicit relationships between blurry and sharp images [12, 26, 38, 39, 49]. Despite their high performance on existing public datasets, these learning-based methods often fail when facing extreme blur conditions or on real-world blurry images. The performance of these methods heavily relies on the quality and scale of the training data, which creates the need for a more general and reliable deblurring method.

Event camera [5, 11, 29] is a kind of bio-inspired asynchronous sensor with high temporal resolution (in the order of μs) and high dynamic range. Different from traditional frame-based cameras, it captures the intensity change of each pixel (*i.e.*, the *event* information) independently if the change surpasses a threshold. Event cameras encode the intensity change information within the exposure time of the image frame into an event stream, making it possible to deblur an image frame with events [27]. However, because of sensor noise and uncertainty in the aforementioned threshold, it is difficult to use a physical model to deblur images based solely on events. Thus, some methods [14, 23, 34] utilize CNNs to deal with noise corruption and threshold uncertainty. Nevertheless, these methods only achieve slight performance gains compared to image-only methods, due to the choice of inefficient event representations and fusion mechanisms between events and images.

In this paper, we propose MEFNet, a multi-scale event fusion network for image deblurring which effectively combines information from event and frame-based cameras for image deblurring. Motivated by the physical model of event-based image deblurring [27], we design a symmetric cumulative event representation (SCER) specifically for deblurring and formulate a two-stage image restoration model. This model is implemented as a CNN with two branches: an image branch and an event branch. In order to fuse information from the two modalities, we propose an affine event-image fusion module and we fuse representations from the two branches via this module at multiple levels. We also enable information exchange between the two stages of our network by applying event mask gated connections, which selectively transfer feature maps from the encoder and decoder of the first stage to the second stage. A detailed ab-

lation study shows the effectiveness of our model architecture and our proposed modules. Additionally, we record a real-world event blur dataset named High-Quality Blur (HQBlur) in an optical laboratory with stable illumination and a high-precision electronically controlled slide-rail. We conduct extensive comparisons against state-of-the-art deblurring methods on the GoPro dataset [26] with synthetic events and on our HQBlur dataset with real events and demonstrate the superiority of our event-based image deblurring method.

In summary, we make the following contributions:

- We design MEFNet, a novel two-stage end-to-end deblurring network, which is motivated by the physical formulation of motion blur and progressively restores the input image using both image and event inputs.
- We equip MEFNet with a novel symmetric cumulative event voxel representation specifically for deblurring, an affine event-image fusion module incorporated at multiple levels of our network, and event mask gated connections to enable direct information flow from the first to the second stage of the network.
- We record HQBlur, a real-world dataset with blurry images, sharp images and events from an event camera, which provides a challenging evaluation setting for deblurring methods.
- We set the new state of the art for image deblurring with MEFNet on the GoPro dataset and the newly proposed HQBlur dataset.

2. Related Work

Image deblurring. Traditional approaches often formulate deblurring as an optimization problem [10, 16, 17, 21, 22, 46]. Recently, with the success of deep learning, image deblurring achieves impressive performance due to the CNNs. CNN-based methods directly map the blurry image to the latent sharp image. Several novel components and techniques have been proposed, such as attention modules [37, 40], multi-scale fusion [26, 39], multi-stage networks [7, 47], and coarse-to-fine strategies [9], improving the accuracy and robustness of deblurring. Despite the benefits they have shown for deblurring, all aforementioned deep networks operate solely on images, a modality which does not explicitly capture *motion* and thus inherently limits performance when facing real-world blurry images especially in extreme conditions.

Event-based deblurring. Recently, events have been used for motion image deblurring, due to the strong connection they possess with motion information. Pan *et al.* [27] proposed an Event Double Integral (EDI) deblurring model using the double integral of event data. They established a mathematical event-based model mapping blurry frames to sharp frames, which is a seminal approach to deblurring with events. However, limited by the sampling mechanism

of event cameras, this method often introduces strong accumulated noise. Jiang *et al.* [14] extracted motion information and sharp edges from events to assist deblurring with a network. However, they failed to take full advantage of event information, as they performed naive early fusion by merely concatenating events into the main branch of their network. Lin *et al.* [23] fused events with image via dynamic filters from STFAN [51]. In addition, Shang *et al.* [34] fused event information into a weight matrix that can be applied to any state-of-the-art network. To sum up, most of the above event-based learning methods failed to fully exploit event information, achieving only minor improvements compared to state-of-the-art image-only methods on standard benchmarks.

Event representation. Different from synchronous signals like images from frame-based cameras, events are asynchronous and sparse. A key point in how to extract information from events effectively and efficiently is the representation of the events. Event representation is an application-dependent problem and different tasks admit different solutions. The event-by-event method is suitable for spiking neural networks owing to its asynchronous architecture [28, 33, 44]. Time surface, which is a 2-dimension map that stores the time value deriving from the timestamp of the last event, has proved suitable for event-based classification [1, 20, 35]. For modern learning architectures, some works chose to convert events to a 2D frame by counting events or accumulating polarity [24, 25, 34]. This method is comparable for conventional computer vision tasks but loses most of the temporal information. Space-time histograms of events, also called voxel grids, preserve the temporal information of events better by accumulating event polarity on a voxel [4, 52]. For the task of image deblurring, most works utilized 2D event-image pairs [34] or borrowed Stacking Based on Time (SBT) representations from image reconstruction [41]. However, there is still not a representation that is specifically designed for motion deblurring to fully unleash the potential of event information.

3. Method

We first introduce the mathematical model for the formation of blurry images from sharp images that involves events in Sec. 3.1. Based on this model, we pose the event-based deblurring problem as a deblurring-denoising problem. We propose a symmetric cumulative representation for events in Sec. 3.2, which constitutes a 3D voxel grid in which the temporal dimension is discretized. This event representation is provided as input together with the blurry image to our two-stage network, the architecture of which is detailed in Sec. 3.3. In particular, we present (i) our novel affine event-image fusion module, which is introduced at *multiple levels* of our network, and (ii) an event mask gated connection between the two stages of the network, which helps

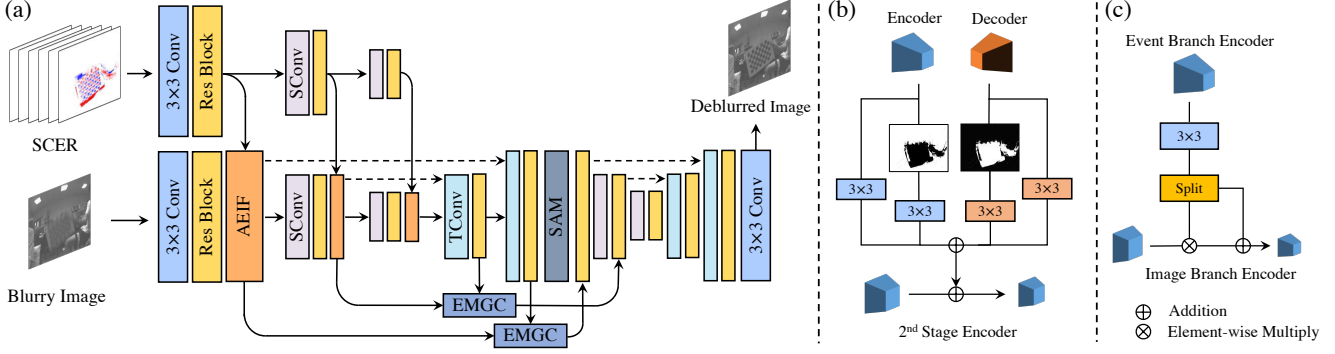


Figure 1. (a): **The architecture of the proposed Multi-scale Event Fusion Network (MEFNet)**. MEFNet consists of two UNet-like backbones [32] and an event extraction branch. After each residual convolution block (Res Block), feature maps from the event branch are fused with feature maps from the image branch. The second UNet backbone refines the deblurred image further. “SCER”, “SConv”, “TConv”, and “SAM” denote Symmetric Cumulative Event Representation, 4×4 strided convolution with stride 2, 2×2 transposed convolution with stride 2, and Supervision Attention Module [47], respectively. (b): **The Event Mask Gated Connection module (EMGC)** transfers feature maps across stages guided by an event mask. (c): **The Affine Event-Image Fusion module (AEIF)** fuses the feature maps from the event branch and the image branch in an affine way.

selectively forward to the second stage the features at sharp regions of the input from the encoder and the features at blurry regions from the decoder of the first stage.

3.1. Problem Formulation

For an event camera, the i -th event e_i is represented as a tuple $e_i = (x_i, y_i, t_i, p_i)$, where x_i , y_i and t_i represent the pixel coordinates and the timestamp of the event respectively. $p_i \in \{-1, +1\}$ is the polarity of the event [5, 29]. An event is triggered at time t only when the change in pixel intensity \mathcal{I} surpasses the threshold compared to the pixel intensity at the time of the last trigger. This is formulated as

$$p_i = \begin{cases} +1, & \text{if } \log \left(\frac{\mathcal{I}_t(x_i, y_i)}{\mathcal{I}_{t-\Delta t}(x_i, y_i)} \right) > c, \\ -1, & \text{if } \log \left(\frac{\mathcal{I}_t(x_i, y_i)}{\mathcal{I}_{t-\Delta t}(x_i, y_i)} \right) < -c, \end{cases} \quad (1)$$

where c is the contrast threshold of intensity change and it may vary across different sensors.

Given the intensity of a latent sharp image \mathbf{L} , according to [27], the corresponding blurred image \mathbf{B} can be derived by the Event-based Double Integral (EDI) model:

$$\begin{aligned} \mathbf{B} &= \frac{1}{T} \int_{f-T/2}^{f+T/2} \mathbf{L}(t) dt \\ &= \frac{\mathbf{L}(f)}{T} \int_{f-T/2}^{f+T/2} \exp \left(c \int_f^t e(s) ds \right) dt, \end{aligned} \quad (2)$$

where f is the middle point of the exposure time T , $e(s)$ is the event stream and $\mathbf{L}(f)$ is the latent sharp image corresponding to the blurred image \mathbf{B} . The discretized version of (2) can be expressed as

$$\mathbf{B} = \frac{\mathbf{L}(N)}{2N+1} \sum_{i=0}^{2N} \exp \left(c \operatorname{sgn}(i-N) \sum_{j: m \leq t_j \leq M} p_j \delta_{x_j y_j} \right), \quad (3)$$

where sgn is the signum function, $m = \min\{f + T/2(i/N - 1), f\}$, $M = \max\{f + T/2(i/N - 1), f\}$ and δ is the Kronecker delta, defined as

$$\delta_{kl}(m, n) = \begin{cases} 1, & \text{if } k = m \text{ and } l = n, \\ 0, & \text{otherwise.} \end{cases} \quad (4)$$

In (3), we partition the exposure time T into $2N + 1$ equal intervals. Rearranging (3) yields:

$$\mathbf{L}(N) = \frac{(2N+1)\mathbf{B}}{\sum_{i=0}^{2N} \exp \left(c \operatorname{sgn}(i-N) \sum_{j: m \leq t_j \leq M} p_j \delta_{x_j y_j} \right)}. \quad (5)$$

Generic form of the network. The formulation in (5) indicates that the latent sharp image can be derived from the blurred image as well as the set of events $\mathcal{E} = \{e_i = (x_i, y_i, t_i, p_i) : f - T/2 \leq t_i \leq f + T/2\}$ (i.e., all the events which are triggered within the exposure time), when events in this set are accumulated over time. We propose to learn this relation with a deep CNN, which admits as inputs the blurred image and the events and maps them to the sharp image. The generic form of the learned mapping is

$$\mathbf{L}_{\text{initial}} = f_3(f_1(\mathbf{B}; \Theta_1), f_2(\mathcal{E}; \Theta_2); \Theta_3), \quad (6)$$

where the blurred image and the events are mapped individually to intermediate representations via f_1 and f_2 respectively and these intermediate representations are afterwards passed to a joint mapping f_3 . Θ_1 , Θ_2 and Θ_3 denote the respective parameters of the three mappings. The main challenges we need to address given this generic formulation of our model are (i) how to represent the set of events \mathcal{E} in a suitable way for inputting it to the CNN, and (ii) how and when to fuse the intermediate representations that are generated for the blurred image by f_1 and for the events by f_2 ,

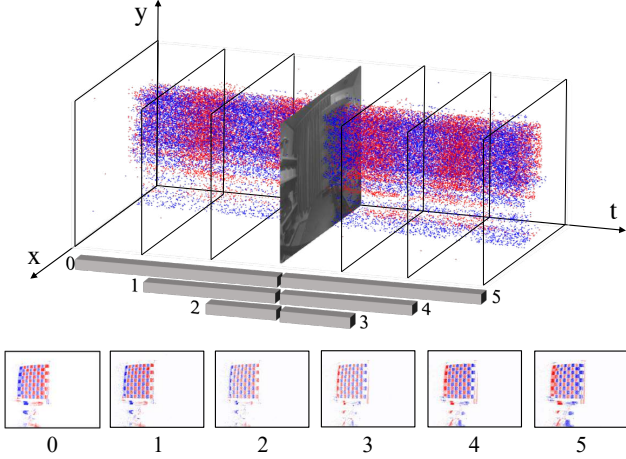


Figure 2. **The proposed Symmetric Cumulative Event Representation (SCER).** Red and blue dots represent events with positive and negative polarity respectively. The bottom part of the figure depicts the individual channels of SCER and the saturation of the dot color represents the relative intensity change corresponding to the central latent sharp frame.

i.e., how to design f_3 . In Sec. 3.2 we address the issue of how to represent the events and in Sec. 3.3, we address the issue of how to perform fusion by properly designing the architecture of our network.

Last but not least, (3) is the ideal formulation for event-based motion image deblur. However, in real-world settings, three factors make it impossible to restore the image simply based on this equation:

- Instead of being strictly equal to a fixed value, the values of threshold c for a given event camera are neither constant in time nor across the image space [36, 43].
- Intensity changes that are lower than the threshold c do not trigger an event.
- Spurious events occur over the entire image.

Most of the restoration errors come from the first two factors, which result in degradation of the restored image in regions with events. We denote these regions as R_e . Taking the above factors into account, we design our network so that it includes a final mapping of the initial deblurred image $\mathbf{L}_{\text{initial}}$ to a denoised version of it, which can correct potential errors in the values of pixels inside R_e :

$$\mathbf{L}_{\text{final}} = f_4(\mathbf{L}_{\text{initial}}; \Theta_4). \quad (7)$$

3.2. Symmetric Cumulative Event Representation

To feed the asynchronous events corresponding to synchronized image frames to our CNN, we design a representation specifically suited for the deblurring setting. In (3), the accumulation of polarities via the inner sum on the right-hand side indicates the relative intensity changes between the target latent sharp image $\mathbf{L}(N)$ and each of the

rest of latent sharp images in the exposure time. The accumulation via the outer sum on the right-hand side represents the sum of all latent sharp images. Based on this relationship, we propose the Symmetric Cumulative Event Representation (SCER). As Fig. 2 shows, the exposure time T of the blurry image is divided equally into $2N$ intervals. Assuming $2N + 1$ latent sharp images in T , the polarity accumulation from the central target latent image $\mathbf{L}(N)$ to a single latent image turns into a 2D tensor with dimensions (H, W) :

$$\mathbf{SCER}_i = \text{sgn}(i - N) \sum_{j: m \leq t_j \leq M} p_j \delta_{x_j y_j}. \quad (8)$$

For $i = N$, $\mathbf{SCER}_N = 0$, so we discard this tensor. The remaining $2N$ tensors are concatenated together, forming a tensor which indicates intensity changes between the central latent sharp image $\mathbf{L}(N)$ and each of the $2N$ other latent images. In this way, $\mathbf{SCER} \in \mathbb{R}^{H \times W \times 2N}$ includes all the relative intensity value corresponding to the center latent sharp frame and it becomes suitable for feature extraction with our CNN-based image deblurring model. As the accumulation limits change, our SCER also contains both information about the area in which blur occurs (channel 0 and channel $2N - 1$) and information about sharp edges (channel $N - 1$ and channel N).

Our method discretizes T into $2N$ parts, quantizing temporal information of events within the time interval $\frac{T}{2N}$. However, SCER still holds temporal information, as the endpoints of the time interval in which events are accumulated is different across channels. The larger the N , the less temporal information is lost. In our implementation, we fix $N = 3$.

3.3. Network Architecture

In this section, we present the Multi-scale Event Fusion Network (MEFNet), which consists of two stages, to progressively restore sharp images from blurred images and event streams. The detailed architecture of MEFNet is illustrated in Fig. 1. Both stages have an encoder-decoder structure. In the first stage, we fuse the event information with the image branch at multiple levels using a novel Affine Event-Image Fusion module. Between the two stages, we design an Event Mask Gated Connection module to boost the feature aggregation with blurring priors from events.

Two-stage backbone. Based on the generic form of the network presented in (6) and (7), we design two sub-networks to progressively restore the blurred image with event information. The two sub-networks are based on the UNet [32] architecture and each sub-network consists of two down-sampling and up-sampling layers. Between the encoder and decoder, we add a skip connection with 3×3 convolution. The residual convolution block in the UNet consists of two 3×3 convolution layers and leaky ReLU functions with a

1×1 convolution shortcut. Recently, the Supervised Attention Module (SAM) in multi-stage methods demonstrated superior capacity in transferring features between different sub-networks [7, 47]. Thus, we use SAM to connect the two stages of our network.

Affine event-image fusion module for multi-scale fusion.

How to jointly extract and fuse information from event streams and images is the key to releasing the potential of event data for image deblurring. Previous work [34] simply multiplies the low-resolution feature maps from these two modalities at the bottleneck of the encoder-decoder architecture. However, this leads to loss of spatial detail due to the several downsampling blocks before fusion. Image deblurring is a position-sensitive task, so preserving fine spatial information of event features is desirable. To utilize event data, we propose to fuse them with image data at multiple scales so as to generate images with fine texture details and well-preserved structure. As shown in Fig. 1(a), the event branch consists of three blocks. The first block generates high-resolution feature maps with accurate spatial information and the last block produces low-resolution feature maps with aggregated information across large regions. These feature maps are fused with the feature maps of the main, image branch with our affine event-image based fusion module (AEIF).

We choose the formulation of this fusion by perceiving the feature maps from the event branch as modulators acting on the feature maps of the image branch. Thus, we select an affine fusion scheme, in order to include both a multiplicative and an additive component in this modulation. More specifically, as illustrated in Fig. 1(c), the feature maps $\mathbf{F}_{ev} \in \mathbb{R}^{H \times W \times C}$ from the event branch generate intermediate feature maps $\mathbf{F}_{mid} \in \mathbb{R}^{H \times W \times 2C}$ with simple $1 \times 1 \times C$ depth-wise convolutions, where $H \times W$ denotes spatial dimensions and C is the number of channels. Then, the features \mathbf{F}_{mid} are split into $\mathbf{F}_{weight} \in \mathbb{R}^{H \times W \times C}$ and $\mathbf{F}_{bias} \in \mathbb{R}^{H \times W \times C}$. Finally, the fused feature maps are obtained by applying a dense affine transformation to the feature maps of the image branch, $\mathbf{F}_{img} \in \mathbb{R}^{H \times W \times C}$, where the parameters of the affine transformation are given by the feature maps of the event branch as

$$\mathbf{F}_{fused} = \mathbf{F}_{img} \odot \mathbf{F}_{weight} + \mathbf{F}_{bias}. \quad (9)$$

Event mask gated connection module. Previous work [30] predicts a mask indicating which areas of an image are severely distorted, but these predicted masks are not completely accurate. Apart from information about intensity changes, event data also contain spatial information about the blurred regions of the input image. Typically, regions in which events occur are more severely degraded in the blurry image. Motivated by this observation, we introduce an Event Mask Gated Connection (EMGC) between the two stages of our network to exploit the spatial configuration

of blurred regions.

In particular, we binarize the sum of the first and last channel of SCER and thus obtain a binary event mask, in which pixels where an event has occurred are set to 0 and the rest are set to 1. As illustrated in Fig. 1(b), EMGC masks out the feature maps of the encoder at regions where the event mask is 0, which are expected to be more blurry, and the feature maps of the decoder at regions where the event mask is 1 (using the complement of the event mask), which are expected to be less blurry. A skip connection is added beside the mask operation. Feature maps with less artifacts in the encoder and better restored feature maps are combined through the event mask gate. In this way, we selectively connect feature maps from the encoder and the decoder of the first stage to the second stage. Besides, EMGC eases the flow of information through the network, as it creates a shortcut through which features can be transferred directly from the first to the second stage.

4. HQBlur Dataset

Almost all event-based motion deblurring methods [6, 14, 23, 34, 45] train models on blurred image datasets such as GoPro [26] with synthetic events from ESIM [31]. Although the contrast value c in the event simulator is a pixel-wise variate, the domain gap still exists because of the background activity noise, dark current noise, false negatives in refractory period, and other factors [3, 36, 43]. Recently, Jiang *et al.* [14] proposed BlurDVS by capturing image and events with slow motion and synthesizing motion blurs by averaging multiple nearby frames. However, motion blur in the ground-truth images is inevitable in this setting and events caused by fast motion are different from those obtained by slow motion because of the false negatives in the refractory period of event cameras [3, 45]. Thus, a large-scale real-world dataset with blurry images, reliable corresponding events, and ground-truth sharp images is missing.

We present a new event-based dataset for deblurring, High-Quality Blur (HQBlur), to provide ground truth for blurry images in a two-shot way. To collect HQBlur, we build an image collection system in a high-precision optical laboratory with highly stable illumination. We fix to the optical table the Insightness Seem 1 event camera, a Dynamic and Active Pixel Vision Sensor (DAVIS) outputting time-aligned 260×360 gray images and event streams. To obtain blurry-sharp image pairs under high-speed motion, we also fix a high-precision electronic-controlled slide-rail system to the optical table. In the first shot, we capture images with motion blur for the pattern on the slide-rail and corresponding event streams. In the second shot, according to the timestamp t_s of the blurry images, we select events within the time range $[t_s - 125\mu s, t_s + 125\mu s]$ and visualize these events in the preview of the sharp image capture program. Referring to the edge information from high-

temporal-resolution events, we can relocate the slide-rail to the coordinate corresponding to the timestamp t_s by an electronic-controlled stepping motor and then capture the latent sharp image. Between two shots, the background is kept static and the illumination is strictly stable.

To enhance the generalization of the network for different objects and moving processes, our dataset includes 12 kinds of linear and nonlinear motions for 3 different moving patterns and for the camera itself. The dataset consists of 36 sequences and 1469 groups of blurry-sharp image pairs with associated events, where 486 pairs are used for training and 983 for testing. We also include an additional set with 4 sequences including extreme blur, without ground truth. Please refer to the supplement for more details on HQBlur.

The rationality and accuracy of our two-shot capturing method can be supported by the following two facts: (1) **Latent sharp image alignment.** The positioning error of the high-precision slide-rail (0.05mm) and the maximum displacement of the pattern within the exposure time corresponds to projected distances of less than one pixel on the sensor in the image plane. (2) **Background consistency.** Due to the highly stable optical laboratory environment, the illumination is strictly constant during the alignment process and the acquisition of blurry images. For the background part of blurry and sharp images in the same pair, PSNR is 44.94, indicating that they are highly consistent.

5. Experiments

5.1. Datasets and Settings

GoPro dataset. We use the GoPro dataset [26], which is widely used in motion deblurring, for training and evaluation. It consists of 3214 pairs of blurry and sharp images with a resolution of 1280×720 and the blurred images are produced by averaging several high-speed sharp images. We first upsample the high-frame-rate sharp image sequences of GoPro from 240 FPS to 960 FPS [13], and use ESIM [31], an open-source event camera simulator, to generate simulated event data. To make the results more realistic, we set the threshold c value randomly for each pixel, following a Gaussian distribution $N(\mu = 0.2, \sigma = 0.03)$.

HQBlur dataset. Before evaluating models trained on GoPro on our HQBlur dataset, in order to close the gap between simulated events and real events, we fine-tune the models on the training set of HQBlur. We then evaluate the fine-tuned models on the test set of HQBlur.

Implementation details. Our network requires no pre-training. We train it on 256×256 crops of the full images in GoPro. For data augmentation, horizontal and vertical flips, random noise and hot pixels in event voxels [36] are applied. We use Adam [15] with an initial learning rate of 2×10^{-4} . We use the cosine learning rate strategy with a minimum learning rate of 10^{-7} . The model is trained with

a batch size of 8 for 300k iterations. Fine-tuning on HQBlur involves 600 iterations, the initial learning rate is 2×10^{-5} and other training configurations are kept the same.

Evaluation protocol. All quantitative comparisons are performed using PSNR and SSIM [42]. Apart from these, we also report the relative reduction in error of the best-performing model for the GoPro benchmark. This is done by converting PSNR to RMSE ($\text{RMSE} \propto \sqrt{10^{-\text{PSNR}/10}}$) and translating SSIM to DSSIM ($\text{DSSIM} = (1 - \text{SSIM})/2$).

5.2. Comparisons with State-of-the-Art Models

We compare our method with state-of-the-art image-only and event-based deblurring methods on GoPro and HQBlur. Since most learning-based methods using events do not have publicly available implementations, in the qualitative comparison part, apart from BHA [27], we compare our method with SRN [39] and HINet [7], the current best model on the GoPro benchmark. To have a fair comparison, we also add event-enhanced versions of these two models by concatenating event voxels and images in the input.

GoPro dataset. We report deblurring results in Table 1. Compared to the best existing image-based method [7] and event-based method [6], our method achieves **2.38 dB** and **2.1dB** improvement in PSNR and 0.011 and 0.035 improvement in SSIM respectively with a low parameter count of 7.5M. Despite utilizing an extra modality, other learning-based methods using events such as D²Nets, LEMD, and ERDNet do not improve significantly upon image-only methods, because of the poor fusion of event and image features. Our model sets the new state of the art in image deblurring, showing that our principled two-stage architecture with multi-level affine fusion releases the potential of event information for this task. Note that by simply including SCER to HINet [7], the resulting enhanced version of it also surpasses the best previous event-based method [6].

We show qualitative results on GoPro in Fig. 3. Results from image-based methods are more blurry, losing sharp edge information. BHA [27] restores edges better but suffers from noise around edges because of the factors described in Sec. 3.1. Learning-based methods using events are not stable due to the poor use of motion information from events. By inputting the concatenation of SCER with the image to SRN+ and HINet+, they both achieve large improvements. However, results from SRN+ include artifacts and noise due to the absence of a second stage in the network that would refine the result. HINet+ produces results with more artifacts, because simply concatenating events and images in the input does not properly fuse the two modalities. Based on the physical model for event deblurring, our MEFNet achieves sharp and faithful results. Both dominant structures and fine details are restored well thanks to the application of fusion at multiple scales.

HQBlur dataset. We report quantitative results on HQBlur



Figure 3. **Visual comparison on the GoPro dataset.** SRN+ and HINet+: event enhanced versions of SRN and HINet respectively. Compared to image-based and event-based state-of-the-art methods, our method restores better fine texture and structural patterns.

in Table 2. Our model outperforms all other methods in this challenging real-world setting. Fig. 4 depicts qualitative results from the test set and the additional set. Even the best image-based method, HINet, shows poor performance on these severe cases of real-world motion blur. Event-based methods are more robust to such adverse conditions and less prone to overfitting on synthetic training data. Results from BHA are sharper, but obvious accumulation noise still exists. Simply concatenating event voxels to a state-of-the-art image-based method improves performance significantly because of the physical basis of our SCER representation but still leads to artifacts and ghost structures. Our method restores both smooth texture and sharp edges, demonstrating the superiority of our two-stage architecture and our multi-level event-image affine fusion. Thanks to the selective feature connection via our EMGC module, MEFNet demonstrates restores blurry regions well while also maintaining the content of sharp regions. Results on more images are provided in the supplement.

5.3. Ablation Study

We conduct ablation experiments to analyze the contribution of different components of our model and of our event representation. These experiments are performed on GoPro and they are presented in Tables 3 and 4.

Multi-scale affine fusion. Our AEIF module fuses event and image features effectively, improving PSNR by 0.31 dB compared to simple addition. Performing fusion at multiple levels both preserves fine spatial texture and utilizes rich semantic content, resulting in an improvement of 0.31 dB.

Table 1. **Comparison of motion deblurring methods on the GoPro dataset [26].** † denotes event-based methods. SRN+ and HINet+ denote the event-enhanced versions of SRN and HINet.

Method	PSNR	SSIM
DeblurGAN [18]	28.70 (52.1%)	0.858 (78.9%)
BHA [†] [27]	29.06 (50.1%)	0.940 (50.0%)
Nah <i>et al.</i> [26]	29.08 (49.9%)	0.914 (65.1%)
DeblurGAN-v2 [19]	29.55 (47.2%)	0.934 (54.6%)
SRN [39]	30.26 (42.7%)	0.934 (54.6%)
SRN+ [†]	31.02 (37.4%)	0.936 (53.1%)
DMPHN [48]	31.20 (36.1%)	0.940 (50.0%)
D ² Nets [†] [34]	31.60 (33.1%)	0.940 (50.0%)
LEMD [†] [14]	31.79 (31.6%)	0.949 (41.2%)
Suin <i>et al.</i> [37]	31.85 (31.1%)	0.948 (42.3%)
SPAIR [30]	32.06 (29.5%)	0.953 (36.2%)
MPRNet [47]	32.66 (24.4%)	0.959 (26.8%)
HINet [7]	32.71 (24.0%)	0.959 (26.8%)
ERDNet [†] [6]	32.99 (21.5%)	0.935 (53.9%)
HINet+ [†]	33.69 (14.9%)	0.961 (23.1%)
MEFNet (Ours)[†]	35.09 (0.0%)	0.970 (0.0%)

Table 2. **Comparison of motion deblurring methods on our HQBlur dataset.** The notation is the same as in Table 1.

Method	PSNR	SSIM
SRN	35.10 (30.9%)	0.961 (38.5%)
HINet	35.58 (27.0%)	0.965 (31.4%)
BHA [†] [27]	36.52 (18.6%)	0.964 (33.3%)
SRN+ [†]	36.87 (15.3%)	0.970 (20.0%)
HINet+ [†]	37.68 (7.0%)	0.973 (11.1%)
MEFNet (Ours)[†]	38.31 (0.0%)	0.976 (0.0%)

Two-stage architecture with EMGC. By progressively restoring the blurry image, our two-stage architecture re-

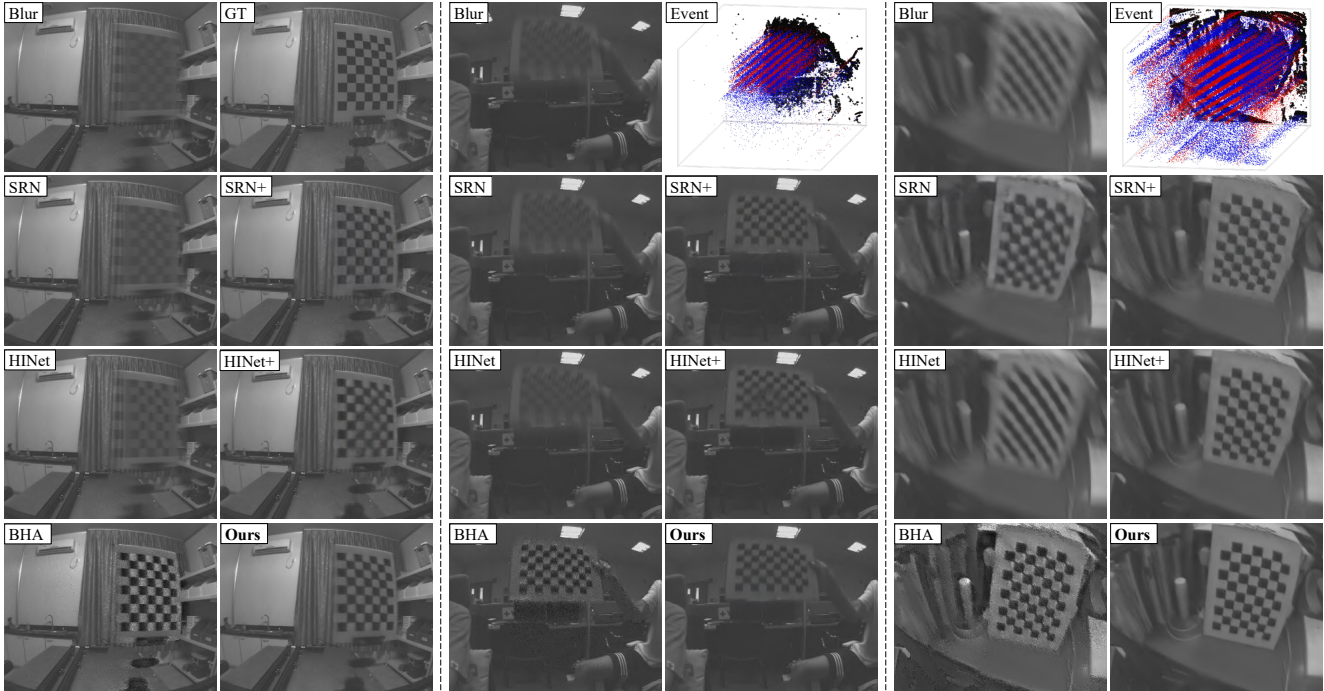


Figure 4. **Visual comparison on the HQBlur dataset.** The first two columns are from the test set of HQBlur dataset, and the rest are from the additional set, for which ground truth is not available. Our method shows superior performance in cases with severe blur both due to object motion and due to camera motion. Best viewed on a screen and zoomed in.

finer details of the deblurred image with events and addresses the noise introduced by the events. Thus, our architecture gives a significant performance boost of 1.14 dB in PSNR and 0.011 in SSIM compared to using a one-stage network. Besides, EMGC between the two stages improves the selective flow of information from the first stage to the second one, yielding an improvement of 0.14 dB.

Event representation. The introduction of event information improves the performance of models due to the high-temporal-resolution intensity change information in events, which provides a vital signal for deblurring. Table 4 shows comparison between SCER and other event representations. Explicitly based on physics, SCER utilizes event information for image deblurring (35.09dB) better compared to the best previous event representation SBT [41] (34.80 dB). Note that simply accumulating all events in the exposure time deteriorates the performance compared to not using events at all, which demonstrates that finding a suitable representation for events in the context of deblurring, such as SCER, is highly non-trivial.

6. Conclusion

In this work, we have looked into single image motion deblurring from the perspective of multi-scale fusion with events. Based on the common physical model which describes both blurry image formation and event generation, we have introduced a two-stage end-to-end motion deblur-

Table 3. **Ablation study on different architectural components of our method** on the GoPro [26] dataset. * denotes single affine fusion at the bottleneck of the encoder-decoder model.

Architecture	Event	EMGC	Fusion	PSNR	SSIM
1-Stage	✗	-	-	29.06	0.936
1-Stage	✓	-	Affine	33.95	0.959
2-Stage	✗	✗	-	32.15	0.954
2-Stage	✓	✗	Affine	34.95	0.967
2-Stage	✓	✓	Concatenate	34.80	0.968
2-Stage	✓	✓	Multiply	34.86	0.968
2-Stage	✓	✓	Add	34.78	0.968
2-Stage	✓	✓	Affine*	34.78	0.967
2-Stage	✓	✓	Affine	35.09	0.970

Table 4. **Comparison between different event representations** on the GoPro [26] dataset. Image denotes feeding the image to the event branch. Stack denotes accumulating events in one channel.

Representation	Image	Stack	SBT [41]	Ours
PSNR	32.14	31.13	34.80	35.09
SSIM	0.954	0.941	0.968	0.970

ring network with an efficient event-image fusion module applied at multiple levels of the network. In addition, we have proposed a novel event voxel representation to best utilize event information for deblurring. We have captured a new real-world dataset, HQBlur, including several cases of severe motion blur, which provides a challenging evaluation setting. The proposed method significantly surpasses prior state-of-the-art in image deblurring both on the GoPro dataset and on our new established HQBlur dataset.

Acknowledgements. This work was partly supported by China Scholarship Council and Sunny Optical Technology (Group) Co., Ltd.

References

- [1] Md Atiqur Rahman Ahad, Joo Kooi Tan, Hyungseop Kim, and Seiji Ishikawa. Motion history image: its variants and applications. *Machine Vision and Applications*, 2012. 2
- [2] Yuval Bahat, Netalee Efrat, and Michal Irani. Non-uniform blind deblurring by reblurring. In *ICCV*, 2017. 1
- [3] R. Baldwin, Mohammed Almatrafi, Vijayan Asari, and Keigo Hirakawa. Event probability mask (EPM) and event denoising convolutional neural network (EDnCNN) for neuromorphic cameras. In *CVPR*, 2020. 5
- [4] Patrick Bardow, Andrew J. Davison, and Stefan Leutenegger. Simultaneous optical flow and intensity estimation from an event camera. In *CVPR*, 2016. 2
- [5] Christian Brandli, Raphael Berner, Minhao Yang, Shih-Chii Liu, and Tobi Delbruck. A 240×180 130 db $3 \mu\text{s}$ latency global shutter spatiotemporal vision sensor. *IEEE Journal of Solid-State Circuits*, 2014. 1, 3
- [6] Haoyu Chen, Minggui Teng, Boxin Shi, Yizhou Wang, and Tiejun Huang. Learning to deblur and generate high frame rate video with an event camera. *arXiv preprint arXiv:2003.00847*, 2020. 5, 6, 7
- [7] Liangyu Chen, Xin Lu, Jie Zhang, Xiaojie Chu, and Chengpeng Chen. HINet: Half instance normalization network for image restoration. In *CVPRW*, 2021. 2, 5, 6, 7, 12, 13, 14, 15, 16
- [8] Sunghyun Cho and Seungyong Lee. Fast motion deblurring. *ACM Transactions on Graphics*, 2009. 1
- [9] Sung-Jin Cho, Seo-Won Ji, Jun-Pyo Hong, Seung-Won Jung, and Sung-Jea Ko. Rethinking coarse-to-fine approach in single image deblurring. In *ICCV*, 2021. 2
- [10] Rob Fergus, Barun Singh, Aaron Hertzmann, Sam T. Roweis, and William T. Freeman. Removing camera shake from a single photograph. *ACM Transactions on Graphics*, 2006. 1, 2
- [11] Guillermo Gallego, Tobi Delbruck, Garrick Michael Orchard, Chiara Bartolozzi, Brian Taba, Andrea Censi, Stefan Leutenegger, Andrew Davison, Jorg Conradt, Kostas Daniilidis, et al. Event-based vision: A survey. *IEEE Transactions on Pattern Analysis and Machine Intelligence*, 2020. 1
- [12] Dong Gong, Jie Yang, Lingqiao Liu, Yanning Zhang, Ian Reid, Chunhua Shen, Anton Van Den Hengel, and Qinfeng Shi. From motion blur to motion flow: A deep learning solution for removing heterogeneous motion blur. In *Proceedings of the IEEE conference on computer vision and pattern recognition*, pages 2319–2328, 2017. 1
- [13] Zhewei Huang, Tianyuan Zhang, Wen Heng, Boxin Shi, and Shuchang Zhou. RIFE: Real-time intermediate flow estimation for video frame interpolation. *arXiv preprint arXiv:2011.06294*, 2020. 6
- [14] Zhe Jiang, Yu Zhang, Dongqing Zou, Jimmy Ren, Jiancheng Lv, and Yebin Liu. Learning event-based motion deblurring. In *CVPR*, 2020. 1, 2, 5, 7
- [15] Diederik P. Kingma and Jimmy Ba. Adam: A method for stochastic optimization. In *ICLR*, 2015. 6
- [16] Jan Kotera, Filip Šroubek, and Peyman Milanfar. Blind deconvolution using alternating maximum a posteriori estimation with heavy-tailed priors. In *CAIP*, 2013. 1, 2
- [17] Dilip Krishnan, Terence Tay, and Rob Fergus. Blind deconvolution using a normalized sparsity measure. In *CVPR*, 2011. 1, 2
- [18] Orest Kupyn, Volodymyr Budzan, Mykola Mykhailych, Dmytro Mishkin, and Jiří Matas. DeblurGAN: Blind motion deblurring using conditional adversarial networks. In *CVPR*, 2018. 7
- [19] Orest Kupyn, Tetiana Martyniuk, Junru Wu, and Zhangyang Wang. DeblurGAN-v2: Deblurring (orders-of-magnitude) faster and better. In *ICCV*, 2019. 7
- [20] Xavier Lagorce, Garrick Orchard, Francesco Galluppi, Bertram E. Shi, and Ryad B. Benosman. HOTS: A hierarchy of event-based time-surfaces for pattern recognition. *IEEE Transactions on Pattern Analysis and Machine Intelligence*, 2017. 2
- [21] Anat Levin, Yair Weiss, Fredo Durand, and William T. Freeman. Understanding and evaluating blind deconvolution algorithms. In *CVPR*, 2009. 1, 2
- [22] Anat Levin, Yair Weiss, Fredo Durand, and William T. Freeman. Efficient marginal likelihood optimization in blind deconvolution. In *CVPR*, 2011. 1, 2
- [23] Songnan Lin, Jiawei Zhang, Jinshan Pan, Zhe Jiang, Dongqing Zou, Yongtian Wang, Jing Chen, and Jimmy Ren. Learning event-driven video deblurring and interpolation. In *ECCV*, 2020. 1, 2, 5
- [24] Min Liu and Tobi Delbruck. Adaptive time-slice block-matching optical flow algorithm for dynamic vision sensors. In *BMVC*, 2018. 2
- [25] Ana I. Maqueda, Antonio Loquercio, Guillermo Gallego, Narciso García, and Davide Scaramuzza. Event-based vision meets deep learning on steering prediction for self-driving cars. In *CVPR*, 2018. 2
- [26] Seungjun Nah, Tae Hyun Kim, and Kyoung Mu Lee. Deep multi-scale convolutional neural network for dynamic scene deblurring. In *CVPR*, 2017. 1, 2, 5, 6, 7, 8
- [27] Liyuan Pan, Cedric Scheerlinck, Xin Yu, Richard Hartley, Miaomiao Liu, and Yuchao Dai. Bringing a blurry frame alive at high frame-rate with an event camera. In *CVPR*, 2019. 1, 2, 3, 6, 7, 12, 13, 14
- [28] Federico Paredes-Vallés, Kirk Y. W. Scheper, and Guido C. H. E. de Croon. Unsupervised learning of a hierarchical spiking neural network for optical flow estimation: From events to global motion perception. *IEEE Transactions on Pattern Analysis and Machine Intelligence*, 2020. 2
- [29] Lichtsteiner Patrick, Christoph Posch, and Tobi Delbruck. A 128×128 120 db $15 \mu\text{s}$ latency asynchronous temporal contrast vision sensor. *IEEE Journal of Solid-State Circuits*, 2008. 1, 3
- [30] Kuldeep Purohit, Maitreya Suin, A. N. Rajagopalan, and Vishnu Naresh Boddeti. Spatially-adaptive image restoration using distortion-guided networks. In *ICCV*, 2021. 5, 7

- [31] Henri Rebecq, Daniel Gehrig, and Davide Scaramuzza. ESIM: an open event camera simulator. In *CoLR*, 2018. 5, 6, 12
- [32] Olaf Ronneberger, Philipp Fischer, and Thomas Brox. U-Net: Convolutional networks for biomedical image segmentation. In *MICCAI*, 2015. 3, 4
- [33] Cedric Scheerlinck, Nick Barnes, and Robert Mahony. Continuous-time intensity estimation using event cameras. In *ACCV*, 2018. 2
- [34] Wei Shang, Dongwei Ren, Dongqing Zou, Jimmy S. Ren, Ping Luo, and Wangmeng Zuo. Bringing events into video deblurring with non-consecutively blurry frames. In *ICCV*, 2021. 1, 2, 5, 7
- [35] Amos Sironi, Manuele Brambilla, Nicolas Bourdis, Xavier Lagorce, and Ryad Benosman. HATS: Histograms of averaged time surfaces for robust event-based object classification. In *CVPR*, 2018. 2
- [36] Timo Stoffregen, Cedric Scheerlinck, Davide Scaramuzza, Tom Drummond, Nick Barnes, Lindsay Kleeman, and Robert Mahony. Reducing the sim-to-real gap for event cameras. In *ECCV*, 2020. 4, 5, 6
- [37] Maitreya Suin, Kuldeep Purohit, and A. N. Rajagopalan. Spatially-attentive patch-hierarchical network for adaptive motion deblurring. In *CVPR*, 2020. 2, 7
- [38] Jian Sun, Wenfei Cao, Zongben Xu, and Jean Ponce. Learning a convolutional neural network for non-uniform motion blur removal. In *Proceedings of the IEEE Conference on Computer Vision and Pattern Recognition*, pages 769–777, 2015. 1
- [39] Xin Tao, Hongyun Gao, Xiaoyong Shen, Jue Wang, and Jiaya Jia. Scale-recurrent network for deep image deblurring. In *CVPR*, 2018. 1, 2, 6, 7, 12, 13, 14, 15, 16
- [40] Fu-Jen Tsai, Yan-Tsung Peng, Yen-Yu Lin, Chung-Chi Tsai, and Chia-Wen Lin. BANet: Blur-aware attention networks for dynamic scene deblurring. *arXiv preprint arXiv:2101.07518*, 2021. 2
- [41] Lin Wang, S. Mohammad Mostafavi I., Yo-Sung Ho, and Kuk-Jin Yoon. Event-based high dynamic range image and very high frame rate video generation using conditional generative adversarial networks. In *CVPR*, 2019. 2, 8
- [42] Zhou Wang, Alan C. Bovik, Hamid R. Sheikh, and Eero P. Simoncelli. Image quality assessment: from error visibility to structural similarity. *IEEE Transactions on Image Processing*, 2004. 6
- [43] Ziwei Wang, Yonhon Ng, Pieter van Goor, and Robert Mahony. Event camera calibration of per-pixel biased contrast threshold. In *ACRA*, 2019. 4, 5
- [44] David Weikersdorfer and Jörg Conradt. Event-based particle filtering for robot self-localization. In *ROBIO*, 2012. 2
- [45] Fang Xu, Lei Yu, Bishan Wang, Wen Yang, Gui-Song Xia, Xu Jia, Zhendong Qiao, and Jianzhuang Liu. Motion deblurring with real events. In *ICCV*, 2021. 5, 12
- [46] Li Xu, Shicheng Zheng, and Jiaya Jia. Unnatural L0 sparse representation for natural image deblurring. In *CVPR*, 2013. 1, 2
- [47] Syed Waqas Zamir, Aditya Arora, Salman Khan, Munawar Hayat, Fahad Shahbaz Khan, Ming-Hsuan Yang, and Ling Shao. Multi-stage progressive image restoration. In *CVPR*, 2021. 2, 3, 5, 7, 11, 12, 13, 14, 15, 16
- [48] Hongguang Zhang, Yuchao Dai, Hongdong Li, and Piotr Koniusz. Deep stacked hierarchical multi-patch network for image deblurring. In *CVPR*, 2019. 7
- [49] Jiawei Zhang, Jinshan Pan, Jimmy Ren, Yibing Song, Linchao Bao, Rynson WH Lau, and Ming-Hsuan Yang. Dynamic scene deblurring using spatially variant recurrent neural networks. In *Proceedings of the IEEE Conference on Computer Vision and Pattern Recognition*, pages 2521–2529, 2018. 1
- [50] Kai Zhang, Wangmeng Zuo, Yunjin Chen, Deyu Meng, and Lei Zhang. Beyond a Gaussian denoiser: Residual learning of deep CNN for image denoising. *IEEE Transactions on Image Processing*, 2017. 1
- [51] Shangchen Zhou, Jiawei Zhang, Jinshan Pan, Haozhe Xie, Wangmeng Zuo, and Jimmy Ren. Spatio-temporal filter adaptive network for video deblurring. In *ICCV*, 2019. 2
- [52] Alex Zihao Zhu, Liangzhe Yuan, Kenneth Chaney, and Kostas Daniilidis. Unsupervised event-based learning of optical flow, depth, and egomotion. In *CVPR*, 2019. 2

A. More Details on MEFNet

A.1. Supervision Attention Module

To help the second stage of MEFNet also gain access to the input image, we place a supervision attention module [47] between the two stages of MEFNet. As illustrated in Fig. 5, the feature maps from the first stage $F_{in} \in \mathbb{R}^{H \times W \times C}$ first generate a residual image, via a 1×1 convolution. H , W , and C are the height, width, and number of channels. The blurry image is added with the residual image and we obtain the predicted deblurred image from the first stage. Then, after a 1×1 convolution and sigmoid function, the resulting attention maps are added to the identity mapping path. Finally, the output $F_{out} \in \mathbb{R}^{H \times W \times C}$ is concatenated with the feature maps in the second stage.

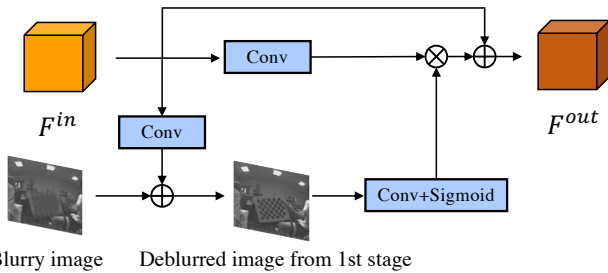


Figure 5. The architecture of the supervision attention module [47].

A.2. Loss Function

We adopt the Peak Signal-to-Noise Ratio (PSNR) loss as the loss function for training our network. The definition of PSNR is:

$$PSNR(x, y) = 20 \log_{10} \frac{MAX}{\sqrt{MSE}}, \quad (10)$$

where MAX is the maximum possible pixel value of the image, and MSE is the mean squared error:

$$MSE = \frac{1}{mn} \sum_{i=0}^{m-1} \sum_{j=0}^{n-1} [x(i, j) - y(i, j)]^2, \quad (11)$$

where m , n are the number of rows and the number of columns in the images x and y , respectively.

The definition of PSNR loss in our model is:

$$Loss = -\frac{1}{2} \sum_{i=1}^2 PSNR(X_i, Y) \quad (12)$$

where X_i is the predicted image of the i -th stage in MEFNet, and Y is the ground-truth image.

Table 5. Detailed information about Insightness Seem 1 camera.

Generation	SEEM1	
Lens	F2.0, 2.5mm, FOV 130°	
Spatial resolution	320 (horizontal) \times 262 (vertical) active pixels	
Optical format	1/3.2 inch, pixel field is centered	
Pixel pitch	13um	
Data type	Change detection events	Image frames
Temporal resolution	Up to 10kHz (configurable)	Up to 30Hz (configurable)
Dynamic range	>98 dB	50 dB
Shutter mode	-	Electronic global shutter
Sensitivity/ Intensity resolution	Configurable threshold down to 50% contrast	10-bit on-chip ADCs
Latency	<1 ms for >150 lux scene illumination <5 ms for >30 lux scene illumination	-
Readout	USB 2.0 and MIPI-CSI 2 (under development)	
Readout bandwidth	~12 Meps (USB 2.0) >40 Meps (MIPI)	

B. More Details on HQBlur dataset

B.1. Event Camera Detail

We choose Insightness Seem 1 camera, which is a Dynamic and Active Pixel Vision Sensor (DAVIS) outputting time-aligned 360×262 gray images and event streams. For the convenience of data processing, we discard the last two columns, so the image size is 360×260 in the dataset. Table 5 shows detailed information about our camera.

B.2. Data Capture

We adopt the two-shot strategy in blurry-sharp image collection. To ensure the motion of the object or the motion of the camera being the only factor that changes in the two shots, we keep the illumination still and other objects in the field of view of the camera still.

In the first shot, we capture images with motion blur for the pattern on the slide-rail and corresponding event streams. In the second shot, according to the timestamp t_s of the blurry images, we select events within the time range $[t_s - 125\mu s, t_s + 125\mu s]$ and visualize these events in the preview of the sharp image capture program. Referring to the edge information from high-temporal-resolution events, we can relocate the slide-rail to the coordinate corresponding to the timestamp t_s by an electronic-controlled stepping motor and then capture the latent sharp image.

Fig. 6 shows blurry images and corresponding sharp ground truth images with visualized events in the time range $[t_s - 125\mu s, t_s + 125\mu s]$. In all sequences, the object movement distance in the direction perpendicular to the optical axis corresponds to a movement distance of less than one pixel on the sensor in the image space.

B.3. Data Categories

We include 12 kinds of linear and nonlinear motions for 3 different patterns, **but the 2 kinds of patterns are not be presented here to maintain anonymity**. HQBlur contains (i) 36 sequences which contain a total of 1469 blurry-sharp

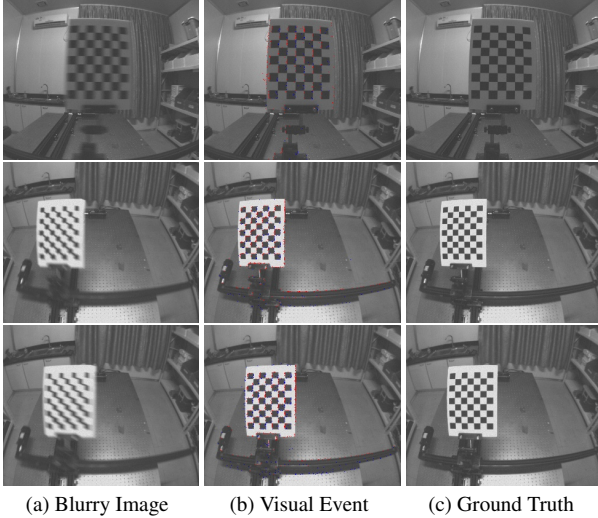


Figure 6. **Example images from the dataset collection procedure for HQBlur.** (a): Blurry images in the first shot. (b): In the second shot, we align the pattern with the visualized events. (c): The captured ground truth.

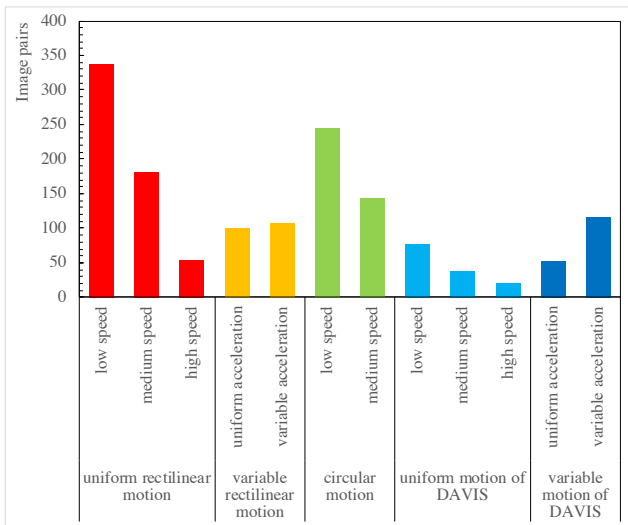


Figure 7. **Diagram of the distribution of categories in HQBlur.** “Low speed”, “medium speed”, and “high speed” equal to $0.325m/s$, $0.75m/s$, and $1.5m/s$, respectively. The accelerate rate equals to $0.75m/s^2$.

image pairs with associated events, where 486 pairs are used for training and 983 for testing, and (ii) 4 sequences from an additional set without ground truth. Fig. 7 shows the exact distribution of all categories.

C. More Qualitative Results

In this section we compare our MEFNet with SRN [39], HINet [7], MPRNet [47], SRN+ (the enhanced version of SRN), HINet+ (the enhanced version of HINet), and

BHA [27]. We show more qualitative results in Fig. 8 and Fig. 9.

C.1. GoPro Dataset

As illustrated in Fig. 8, our method restores the structural elements (*i.e.* numbers, characters, and lines) and detailed textures (*i.e.* face detail). Compared to state-of-the-art image-based and event-based methods, our method achieves better restoration results.

C.2. HQBlur Dataset

Fig. 9 shows more qualitative results from the HQBlur dataset. Image-only methods (SRN [39], HINet [7], MPRNet [47]) perform poorly in such severe blurry conditions. Event-based methods are more robust, but BHA [27] is prone to noise. SRN+ and HINet+ show artifacts because of the insufficient use of event information. Our MEFNet achieves the best performance.

D. Potential Negative Societal Impacts

Since event cameras will likely go to mass production, some of the cell phones may be equipped with this advanced sensor in the near future and our event-based deblurring algorithm may be applied in these cell phones. Our algorithm improves image deblurring performance compared to image-only methods, especially in severe blurry conditions. After mitigating motion blur in the images, one potential negative impact is that intrusive shots are made easier and thus cause bad social effects. This can be alleviated by forcing shutter sound and other methods.

E. Limitations

Although we have achieved impressive deblurring results in most situations, MEFNet also shows performance degradation in the most adverse blurring conditions. Here we show some failure examples on the additional set of the HQBlur dataset in Fig. 10 and Fig. 9 (b).

These are the most severe blur conditions. Even the basic shape of the moving objects cannot be distinguished based only on the blurry image. Although the deblurring performance is not ideal, the basic pattern and shape of the moving object can be recognized. The main reason for failure in these examples is due to the limitation of the hardware: (1) **The temporal resolution of event camera is not enough for such blurry conditions.** This is determined by the event camera itself and the degradation would be alleviated if the hardware improved. (2) **The refractory period makes each pixel not able to react to next intensity changes after last events in a short time,** and this is also a random factor [45]. Because we train models on the synthetic events from ESIM [31], this may be mitigated if more simulation settings are added in ESIM [31].

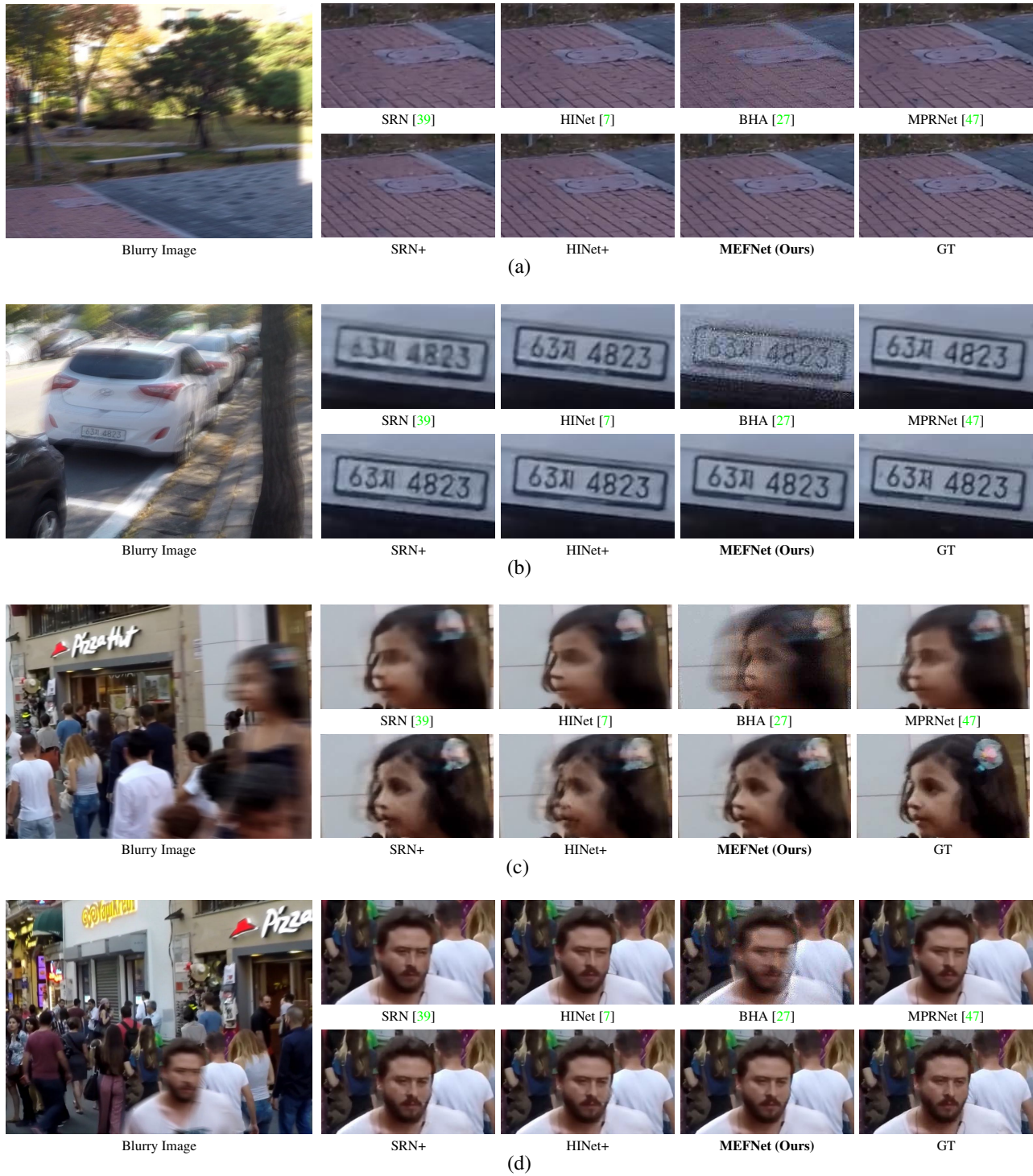


Figure 8. **More visual comparisons on the GoPro dataset.** SRN+ and HINet+: event enhanced versions of SRN [39] and HINet [7] respectively. Our method restores the structural elements (*i.e.* numbers, characters, and lines) and detailed textures (*i.e.* face detail). Compared to state-of-the-art image-based and event-based methods, our method achieves better restoration results. Best viewed on a screen and zoomed in.

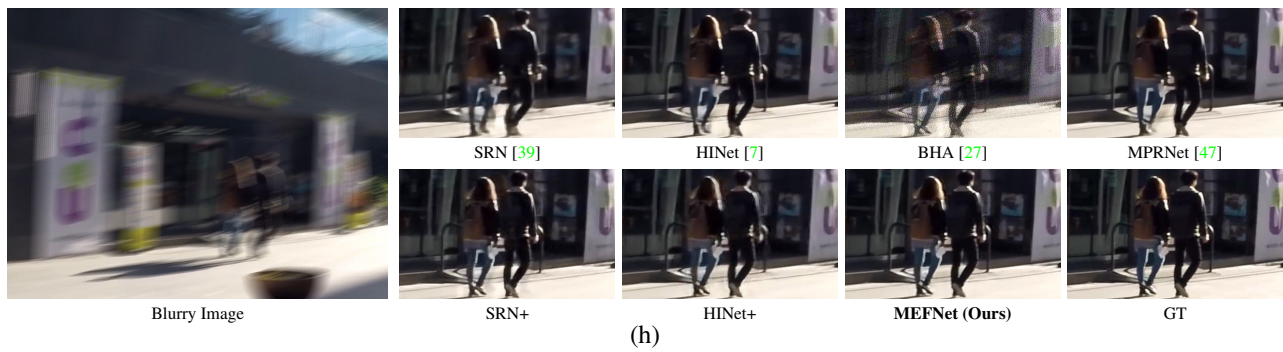
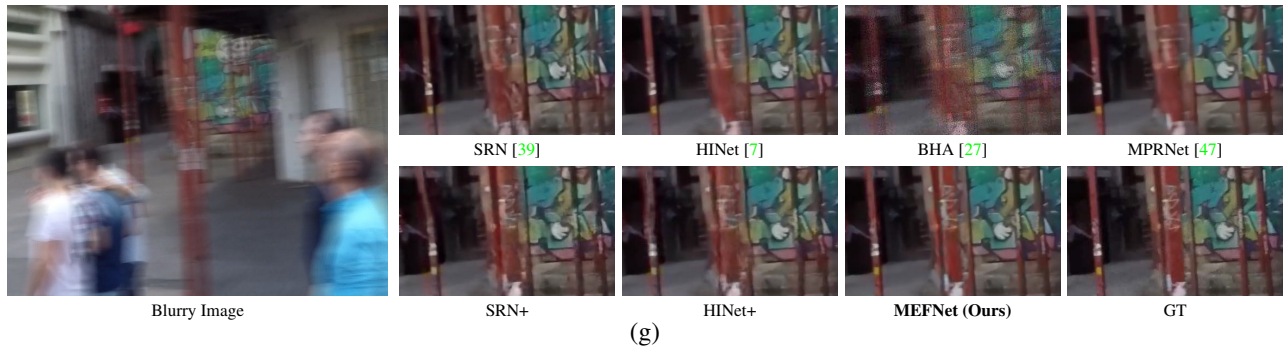
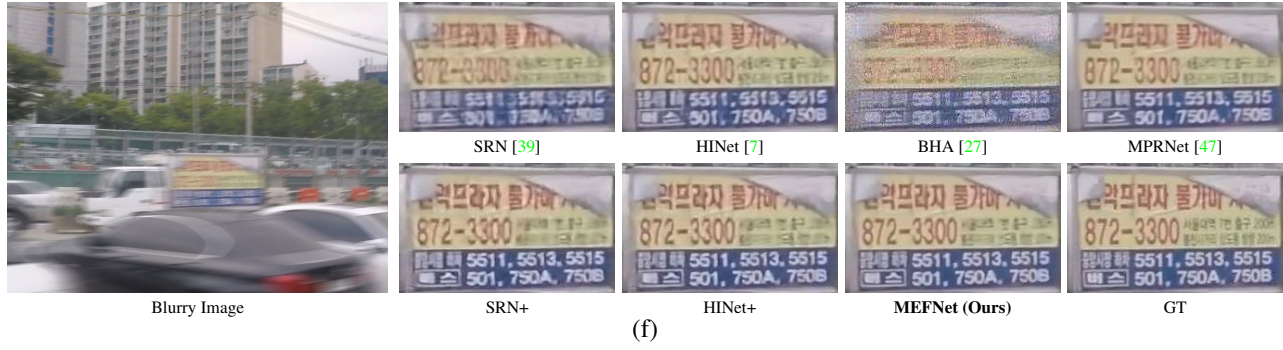
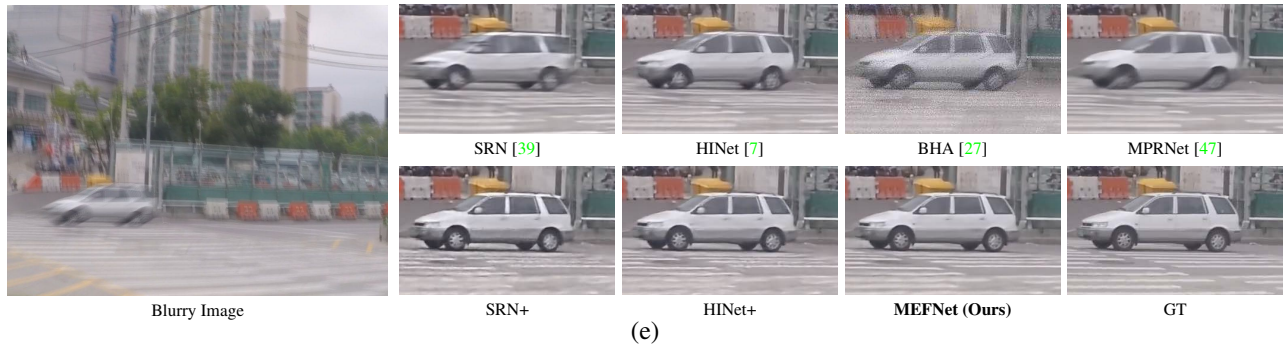


Figure 8. (continued) **More visual comparisons on the GoPro dataset.** SRN+ and HINet+: event enhanced versions of SRN [39] and HINet [7] respectively. Our method restores the structural elements (*i.e.* numbers, characters and lines) and detailed textures (*i.e.* face detail). Compared to image-based and event-based state-of-the-art methods, our method achieves better restoration results. Best viewed on a screen and zoomed in.

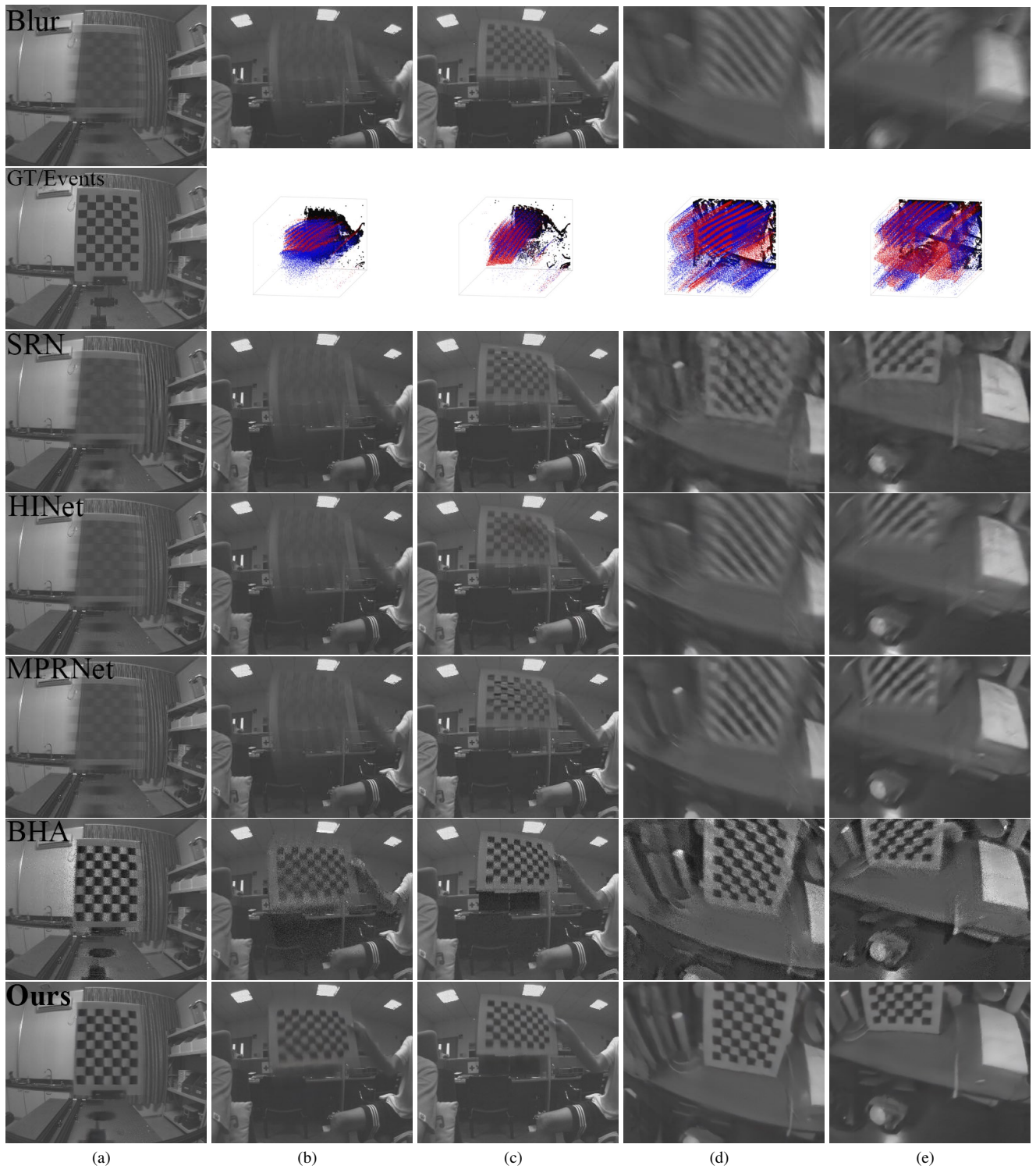


Figure 9. **More visual comparisons on the HQBlur dataset.** SRN+ and HINet+: event enhanced versions of SRN [39] and HINet [7] respectively. (a) is from the test set and (b), (c), (d), and (e) are from the additional set of HQBlur. Image-only methods (SRN [39], HINet [7], MPRNet [47]) perform poorly in such severe blurry conditions. Event-based methods are more robust, and our MEFNet achieves the best performance. Best viewed on a screen and zoomed in.

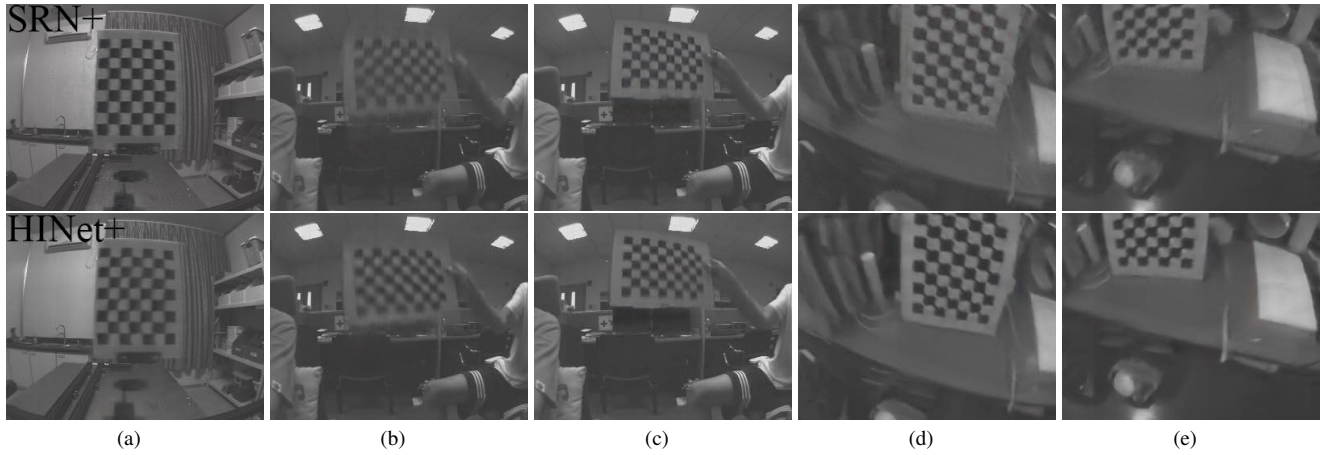


Figure 9. (continued) **More visual comparisons on the HQBlur dataset.** SRN+ and HINet+: event enhanced versions of SRN [39] and HINet [7] respectively. (a) is from the test set and (b), (c), (d), and (e) are from the additional set of HQBlur. Image-only methods (SRN [39], HINet [7], MPRNet [47]) perform poorly in such severe blurry conditions. Event-based methods are more robust, and our MEFNet achieves the best performance. Best viewed on a screen and zoomed in.

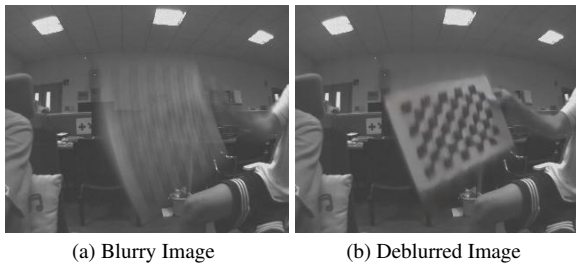


Figure 10. **Failure example in the most severe blur condition.** In the blurry image, the chessboard cannot be delineated. The deblurred image shows some artifacts, and some black squared of the chessboard are merged.